Evaluation of mode II fatigue disbonding using Central Cut Plies specimen and distributed strain sensing technology

Ribeiro, Fabricio N.; Martinez, Marcias; Rans, Calvin

DOI
10.1080/00218464.2018.1433039

Publication date
2019

Document Version
Final published version

Published in
The Journal of Adhesion

Citation (APA)
Ribeiro, F. N., Martinez, M., & Rans, C. (2019). Evaluation of mode II fatigue disbonding using Central Cut Plies specimen and distributed strain sensing technology. *The Journal of Adhesion*, *95*(4), 259-285. https://doi.org/10.1080/00218464.2018.1433039

The Journal of Adhesion

ISSN: 0021-8464 (Print) 1545-5823 (Online) Journal homepage: https://www.tandfonline.com/loi/gadh20

Evaluation of mode II fatigue disbonding using Central Cut Plies specimen and distributed strain sensing technology

Fabricio N. Ribeiro, Marcias Martinez & Calvin Rans

To cite this article: Fabricio N. Ribeiro, Marcias Martinez & Calvin Rans (2019) Evaluation of mode II fatigue disbonding using Central Cut Plies specimen and distributed strain sensing technology, The Journal of Adhesion, 95:4, 259-285, DOI: 10.1080/00218464.2018.1433039

To link to this article: https://doi.org/10.1080/00218464.2018.1433039

Published online: 16 Feb 2018.

THE JOURNAL OF ADHESION
2019, VOL. 95, NO. 4, 259–285
https://doi.org/10.1080/00218464.2018.1433039

Taylor & Francis
Taylor & Francis Group

Evaluation of mode II fatigue disbonding using Central Cut Plies specimen and distributed strain sensing technology

Fabricio N. Ribeiro [a,b], Marcias Martinez [a,c], and Calvin Rans [a]

[a]Faculty of Aerospace Engineering, Delft University of Technology, Delft, The Netherlands; [b]Divisão de Sistemas Aeronáuticos, Instituto de Aeronáutica e Espaço, São José dos Campos, Brazil; [c]Department of Mechanical and Aeronautical Engineering, Clarkson University, Potsdam, NY, USA

ABSTRACT

The lack of a widely-accepted test standard for characterizing the mode II fatigue disbond growth behavior of adhesively bonded interfaces is a challenge to the research community in terms of producing consistent and repeatable results. Typically, researchers apply the End Notch Flexure specimen, which is already used for static delamination studies. However, the needs for static and fatigue disbond growth characterization are not the same, resulting in some undesirable effects in such specimen. This study looks at a particular mode II test configuration known as the Central Cut Plies (CCP) specimen. A critical evaluation of the suitability of this specimen, including the influence of geometry, disbond measurement approaches and the stability of the disbond growth is carried out through a combination of numerical and experimental investigations. A distributed strain sensing system based on Rayleigh Backscattering provided a surface strain profile from which disbond growth rate data was obtained. A finite element model was used to verify the experimental results and determine the disbond length from the strain profiles. Results of this evaluation have shown that the CCP specimen is a promising specimen configuration for characterizing fatigue disbond growth; however, it also presents several challenges that require consideration in its application.

ARTICLE HISTORY
Received 1 November 2017
Accepted 23 January 2018

KEYWORDS
Bonded joints; composites; distributed sensing; Fatigue; mode II

Introduction

Adhesively bonded interfaces present several advantages over classical mechanically fastened joints commonly used in aeronautical structures. The load transfer for bonded interfaces is continuous and does not require fasteners, reducing the overall structural weight. Nevertheless, the certification of bonded primary structures remains a challenge due to the lack of confidence on this type of interfaces and the difficulty in predicting their durability during the aircraft operational service life. Moreover, the typical load condition that adhesively bonded interfaces experience during the operational life is shear (mode II) and, while a static mode II test was already

CONTACT Fabricio N. Ribeiro fabricionr@hotmail.com Faculty of Aerospace Engineering, Delft University of Technology, Delft, The Netherlands.

Color versions of one or more of the figures in the article can be found online at www.tandfonline.com/gadh.

standardized, the scientific community still has not agreed upon on a standard method for testing mode II fatigue for bonded interfaces. In this study, a critical evaluation of the central cut plies (CCP) specimen was performed under mode II disbonding condition. In addition, a novel approach for calculating disbond growth was developed through the use of distributed sensing technology.

The use of adhesively bonded joints brings several advantages to an aircraft structure in comparison to traditional mechanically fastened joints, presenting higher joint stiffness and superior fatigue performance.[1] Another advantage is the weight reduction due to the removal of fasteners, which can save several kilograms when considering a wide body airplane. Moreover, the load is uniformly transferred on a bonded interface, avoiding the stress concentration brought by fasteners and holes.[2] In addition, the removal of fasteners and their corresponding through holes minimizes the problems related to environmental degradation, such as water ingress, humidity and corrosion, while a bonded composite structure behaves as a good protective layer to minimize corrosion on the substrate.[3]

Nevertheless, certification of bonded structures remains difficult. The current accepted means of compliance for the certification of bonded primary structures[4] mandates that limit load capability of a structure must be maintained by one of three means: (i) limiting damage growth (by means of damage arresting features); (ii) proof testing of every production joint; (iii) repeatable and reliable non-destructive assessment of joint residual strength. Reviewing these in reverse order, to the authors' knowledge, there is no certified non-destructive method that can directly assess residual strength. Proof testing is technically possible, but cost-prohibitive when considering the need to test all production joints to their design limit load. Finally, limiting damage growth has resulted in the widespread use of mechanical fasteners to ensure limit load capabilities; the so-called *chicken-riveting* approach. Ideally, the traditional slow damage growth and safety-by-inspection philosophy (otherwise known as Damage Tolerance) adopted for metallic structures could be applied to bonded joints. To enable this, a greater understanding of damage growth in bonded structures is necessary.

For a bonded joint, the bonding interface is expected to be loaded mainly in shear (mode II). Opening loading (mode I) is a detrimental secondary loading that should be minimized during the design process.[5] As a consequence, a well-designed bonded joint usually works in a condition close to pure mode II, commonly above 70%. In such condition, the mode II loading component has a large influence on disbond growth[6,7] and the fracture surface already resembles a pure mode II fracture.[8,9] Thus, it is necessary to perform both static and fatigue tests to characterize the mode II behavior of bonded joints. The static mode II test was vastly investigated[10–14] and a standard test method was established using the

End Notched Flexure (ENF) specimen.[15] On the other hand, for the mode II fatigue testing of bonded joints, there is still no standard test developed up to date. The problem mainly comes with the difficulty in obtaining a specimen with pure shear loading condition that offers a stable disbond growth, and the inability to precisely measure the disbonds developed under such condition. Even so, there are some candidate specimens that can be considered besides ENF. Specimens such as Stabilized End Notched Flexure (SENF)[10,16], Four point End Notched Flexure (4ENF)[13,17], End Loaded Split (ELS)[10,12,18] and Central Cut Plies (CCP)[19–23] have been studied. However, each of these specimens has its own pitfalls related to geometry dependence, stability, frictional influence, starter defect, compliance calculation, data analysis and crack length measurement.[11,18,24]

Among the aforementioned specimens, the Central Cut Plies specimen was chosen for this work due to its characteristics of producing a stable crack growth under fatigue loading and ease of measuring crack growth rate by using a clip extensometer without the need of actually measuring the crack length.[21–23] Another good characteristic of this specimen is the constant crack growth obtained when a constant amplitude cyclic loading is applied under load control. This is a consequence of the strain energy release rate (G) being independent of the crack length under such conditions.[19,20] The constant crack growth rate under constant amplitude loading also makes the specimen a good candidate for studying variable amplitude loading and/or environmental effects, as these effects would be more easily distinguished from the base constant crack growth rate.

The bulk of studies using the CCP specimen available in the literature have focused on delamination growth in composite materials.[19–23,25–28] Although disbond and delamination growth are similar, the larger thickness of adhesive bondlines results in significantly higher fracture toughness. This higher fracture toughness may have an impact on the ideal configuration of the specimen for testing bonded interfaces. For the case of static delamination test, Wisnom[19] and Cui et al.[20] showed preliminary conclusions about the effect of specimen geometry and test parameters on the resulting interlaminar fracture toughness (G_{IIC}). Moreover, Van der Meer and Sluys[26] performed a numerical investigation of the size effect. Scalici et al.[28] presented an experimental and numerical study also regarding the size effect on G_{IIC} and the authors suggested the use of insert films as starting defects for delamination onset in order to remove the influence of the central resin pocket. For the case of fatigue delamination testing, the problems related to delamination onset are avoided by allowing a minimum delamination length to be developed. Thus, Wisnom et al.[21] presented preliminary results on the effect of thickness, cut plies ratio, load frequency, load ratio and cut plies fiber orientation on the fatigue performance of the CCP specimen. These effects, however, have not yet been studied for the case of an adhesive bondline between the continuous and cut plies.

The main objective of this work is to perform a critical evaluation of the Central Cut Plies specimen as a potential candidate for mode II fatigue testing of bonded composite structures. For this evaluation, two main aspects were focused on: (i) assessing the suitability of different measurement techniques for observing disbond growth and (ii) evaluating the influence of specimen geometry and materials on the fatigue testing capabilities. These main aspects are investigated using a combination of experimental, numerical and analytical techniques.

In order to critically evaluate the Central Cut Plies (CCP) specimen, two main aspects related to testing were investigated. First, a critical evaluation of different disbond growth measurement techniques was carried out. A common approach in fracture mechanics specimens is to measure changes in specimen compliance, either through strain and/or total deformation, and relate that to damage size using various assumptions about the damage. Various techniques were evaluated, including the use of a clip extensometer and a surface-mounted distributed sensing optical fiber sensor, and compared to results obtained from ultrasonic C-scan and optical measurement of disbond length. Additionally, finite element modelling was carried out to allow further investigation into the expected relationship between distributed surface strain and disbond size, thus enabling a more critical assessment of the measurement techniques.

The second major aspect investigated was the influence of various specimen parameters on the testing limitations of the CCP specimen. The tensile loading nature of CCP specimen is meant to induce a Mode II disbond between the cut and continuous plies. However, tensile failure of the continuous plies can occur. This was exacerbated by the fact that adhesive bondlines typically have a higher fracture toughness compared to interlaminar delamination planes. This higher fracture toughness means that higher loads are needed for testing bondlines, which increases the possibility for the undesired failure of the adherend. To investigate this aspect, a detailed analytical study on the influence of specimen geometry (particularly the ratio of cut-to-intact plies), composite strength and adhesive fracture toughness on the critical failure mode in the CCP specimen was carried out.

The remainder of this section details the CCP specimen while the next section describes the various measurement techniques, testing methods, finite element models and analytical methods employed to achieve these two goals.

CCP specimen description

The CCP specimen comprises of continuous plies stacked on top and bottom of cut central plies. By applying uniaxial tensile loading to the specimen along its length direction, a transverse crack arises from the resin rich section between the cut plies and it grows within the adhesive layer following the

contour of the central cut plies, forming four cracks. The CCP specimen was mostly used for composite delamination studies. In this case, the four cracks are called delaminations. For the current work, the authors adapted the specimen to a bonded configuration by adding layers of adhesive film between the continuous and cut plies. In this manner, instead of delaminations, four disbonds of length a arise, as indicated in Figure 1. As a result, a pure mode II condition is obtained[20] between the continuous and cut plies. Throughout the remainder of this article, the expression 'delamination' will be used when referring to cases where the specimen was used to study composite delamination and the expression 'disbond' will be used for adhesively-bonded joint configuration. For both cases, the length of the disbond/delamination will be referred to as a. The delamination or disbond onset could be facilitated by use of insert films. In this work, the authors preferred to avoid the use of insert films and rely on naturally formed disbonds, since the specimen geometry with cut plies already facilitates disbond onset.

The resulting expression for the strain energy release rate, G, obtained for the CCP specimen through simple beam theory is given by Equation (1), where P is the applied tensile load, E is the elastic modulus in the longitudinal direction, B is the specimen width, t is the total thickness and χ is the cut plies ratio, calculated by the number of cut plies divided by the total number of composite plies. The expression was initially obtained by Wisnom[19,29], following the methodology proposed by Williams.[30] It should be highlighted that the equation was initially used for delamination studies and it considers the stiffness and total thickness of the composite. For adhesively-bonded specimens, one must take care in correctly accounting for the influence of the adhesive layers on the specimen stiffness, E, and specimen thickness, t. The authors suggest neglecting the contribution of the adhesive layer to both terms (as its stiffness is typically an order of magnitude lower than the composite) and using E and t measured for the composite layers only.

$$G = \frac{P^2}{4EB^2t}\left(\frac{\chi}{1-\chi}\right) \tag{1}$$

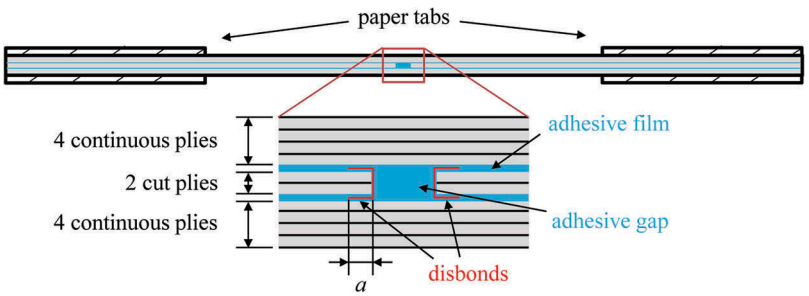

Figure 1. Side view representation of the adhesively-bonded Central Cut Plies specimen with four disbonds.

Equation (1) assumes that all four disbonds grow equally along the specimen's length and symmetric across the specimen mid-plane. Additionally, the equation is applicable only after the disbonds have grown a minimum length from the cut. Cui et al.[20] performed numerical simulations and showed that this minimum length is equivalent to less than four times the total thickness of the internal cut plies. Moreover, Kawashita et al.[25] obtained a minimum length of five to eight times the cut plies thickness utilizing cohesive elements in their model. Regarding the non-symmetrical growth of disbonds, Pascoe et al.[31] studied the occurrence of such condition on thick adherend disbond tests with fiber-metal laminates (Glare) on several specimen configurations that behave similar to the CCP specimen. It was observed that the non-symmetrical condition affects significantly the scatter in the results of disbond growth for thick adherends. By use of a finite element analysis, Pascoe et al. evaluated the impact of several unequal disbond length cases on the maximum strain energy release rate calculated for each disbond. The results showed a negligible difference on the strain energy release rate when the disbond lengths are unequal in the same plane.

Even though the CCP specimen configuration presents four different delaminations/disbonds, it has one big advantage. The resulting range of strain energy release rate (ΔG) obtained with cyclic fatigue loading under load control mode is a function of geometry, material properties and loading only. The ΔG is independent on the disbond length (a). Therefore, a constant ΔG will be obtained for a given constant amplitude loading. Considering a fatigue delamination/disbond growth model where the stable growth region is described by a Paris-Erdogan type of equation, such model can be generally described by Equation (2). As a result, a constant amplitude fatigue cycle applied to the CCP specimen will generate a constant delamination/disbond growth rate (da/dN). On this work, ΔG is calculated according to Equation (3), following the similitude concept described by Rans et al.[32] This fact is not only advantageous to study changes in delamination/disbond growth due to the effects of variable amplitude loading but it also increases the accuracy on the calculation of ΔG, since this calculation will not include the common scatter found in the measurements of mode II delamination/disbond length.

$$\frac{da}{dN} = C(\Delta G)^n \tag{2}$$

$$\Delta G = \left(\sqrt{G_{\max}} - \sqrt{G_{\min}}\right)^2 \tag{3}$$

A consequence of having a constant ΔG for a constant amplitude loading is that it requires changes in the load cycle in order to obtain different ΔG values. It is thus necessary to test the specimen at different constant load cycles to obtain the parameters C and n on Equation (2). However, the maximum ΔG that can

be achieved with a CCP specimen with defined material and geometry will be limited by the maximum load the specimen can handle before achieving static failure. Thus, the static failure of the specimen will determine the maximum load and consequently the maximum ΔG allowed in fatigue tests. On the other hand, the constant and stable delamination/disbond growth observed in the specimen makes it simple to apply several blocks of constant amplitude fatigue cycles in order to obtain several da/dN vs. ΔG data with the same specimen if enough disbond growth is considered for each block.

The use of the CCP specimen for fatigue tests under displacement control does not lead to a constant disbond growth since the ΔG will be dependent of the disbond length. Thus, the displacement control mode presents a need for measuring the disbond length in order to calculate the strain energy release rate, which brings all the uncertainties and difficulties related to the measurement of disbond length under pure mode II condition. These difficulties are discussed in the following section and they are mainly related to the fact that the disbond under mode II is not opened (ie: the crack flanks remain in contact with each other), complicating visual observations of disbond length and growth. The lack of a consistent method to measure disbond length on mode II test specimens can be a major source of the scatter in test results typically observed within the literature. Moreover, many different fatigue specimens such as the DCB (double cantilever beam) and ENF rely on an accurate measurement of the crack length in order to calculate both the crack growth rate and the strain energy release rate. As a consequence, the typical da/dN vs. ΔG plot brings the measurement uncertainties to both axes, resulting in considerable scatter.

Methodology

For the current work, fatigue tests were performed using CCP specimens. In this section, testing methods, finite element models and analytical methods are described. Prior to that, some points of concern are discussed regarding disbond measurement techniques.

Considerations about disbond measurement techniques

A typical method for measuring delamination or disbond length on fatigue test specimens is to perform optical/visual inspection on painted surfaces from the side of the specimen by means of cameras or travelling microscope.[23,33,34] This method works well for an opening mode disbond (mode I) as it is easier to identify the disbond tip. As it relates to mode II disbond, the process is not straightforward and the measurement is difficult, as the adherends remain in contact. The mode II disbond development follows a different process than mode I[9,35], and as a consequence, it is more difficult and ambiguous to define and observe a disbond tip. Several authors reported the difficulty on measuring

mode II delaminations/disbonds through visual inspection[10,21,36,37] and as such, most of them suggest the use of compliance method as an indirect means of obtaining the delamination/disbond length. Other authors[31] observed the same difficulties when observing optically the disbond growth of bonded repairs and highlighted the poor quality of the disbond length measurements. An alternative way to overcome this issue is to choose a specimen that has the compliance varying linearly with the disbond length, for which disbond length can be estimated from the displacement measurements.[38]

The use of compliance to back-calculate disbond length is a common approach used on several different tests. The method relies on the assumption that the compliance changes due to disbond growth only, although other aspects such as matrix cracking or temperature effects can also affect the compliance. Thus, it is an indirect way of obtaining the disbond length. The efficiency of the method was evaluated by Mall et al.[39] whose results were in agreement with both the isochromatic fringes technique obtained from photoelastic material bonded to the lap adherend and the X-Ray technique using dye penetrant zinc iodine. Wisnom et al.[21] used the compliance method with simple beam theory and clip extensometer measurements to obtain the average delamination length of the CCP specimen. The authors observed a very good linear relationship between the loss of stiffness and the delamination growth, except for a small deviation at the beginning of the fatigue test. Allegri et al.[22] applied the same approach and analyzed the accuracy of the method in comparison with microscopy inspection. Allegri et al. calculated a standard error of 130 μm on delamination length measurement for the test setup and concluded that the reliability of the method was good. Rans et al.[23] used this method and observed a considerable difference between visual measurements and the clip extensometer results. The authors highlighted the influence of the zeroing of the extensometer and load cell on these differences. Nevertheless, Rans et al. showed that the rate of delamination growth calculated through Equation (4) was reliable and consistent with visual measurements. In Equation (4), L_{gauge} is the clip extensometer length and ε^* is the measured strain. Rans et al. also analyzed the effects of measurements errors on the calculation strain energy release rate and delamination growth rate by Equations (1,4) respectively and concluded that the errors are in the same order of magnitude and much smaller than the scatter in da/dN observed during tests.

$$\frac{da}{dN} = \frac{1-\chi}{\chi}\left(\frac{EBtL_{gauge}}{2P}\right)\frac{d\varepsilon^*}{dN} \tag{4}$$

Additionally, there are alternative methods to monitor delamination or disbond growth.[40–44] Among several possibilities, an interesting approach uses back-face strain measurements and correlates them to the damage evolution.[45,46] This method presented some improvements with the use of

fiber optics and distributed strain sensing technology[47–51] and it seems to give valuable information about damage evolution on bonded joints.

For this work, the compliance method using a clip extensometer was used to calculate the disbond growth rate of CCP specimens along with a back-face strain measurement technique using optical fibers. The back-face strain method consists in measuring the strain distribution over the specimen surface and calculating the disbond growth from the evolution of the strain profiles. The strain profiles were measured with a distributed fiber optic sensing system based on Rayleigh Backscattering. From the strain profiles, a new method for obtaining disbond growth was developed. A constant strain level was defined and the distance in which the strain profiles crossed the selected strain level was used to obtain the disbond growth. Both clip extensometer and distributed strain results were compared to ultrasonic C-scan and visual inspections. A correlation of the strain profiles and the disbond location was performed with a finite element model.

Experimental setup

The CCP specimens were manufactured from unidirectional carbon-epoxy system Cycom 5276–1 and adhesive film FM 300-2K, both produced by Cytec Industries Inc. (Woodland Park, NJ, USA). The adhesive layers were added between the continuous and cut plies. In this manner, four disbonds developed within the adhesive layers instead of composite delaminations. The specimens were co-cured in order to avoid uncertainties related to surface preparation and bonding procedure. The specimen comprised of 10 composite plies and 2 adhesive films layers, resulting in a 2 cut/8 continuous plies configuration as shown in Figure 1. This configuration was chosen based on previous work from Rans et al.[23] The central cut plies were separated by an adhesive gap of about 10 mm. The composite fiber direction was 0°, aligned with the specimen's length. The specimen's total dimensions were 305 mm length, 25.5 mm width and 1.78 mm thickness. The adhesive layer thickness was 0.17 mm. Paper tabs were glued to the specimen in order to provide a better grip. The mechanical properties for the selected materials are described in Table 1.

Table 1. Mechanical properties of composite and adhesive at 24°C.

Material	Property	Unit	Value
Carbon/epoxy UD	0° Young Modulus, E_{11}	GPa	156.7
Cytec Cycom 5276–1	90° Young Modulus, E_{22}	GPa	8.54
	v_{12}	-	0.32
	In-plane Shear Modulus, G_{12}	GPa	4.63
	0° Tensile Strength, σ_{TS}	MPa	2354
Adhesive film	Young Modulus, E	GPa	2.45
Cytec FM 300-2K	v_{12}	-	0.38
	Lap Shear Strength	MPa	43.2

The specimens were subjected to fatigue and static tests. For the fatigue tests, cyclic loading was applied with a MTS servo-hydraulic test frame of 100kN capacity under load control. The fatigue loading comprised of constant amplitude cycles with a maximum load of 42 kN and a load ratio of 0.1. The test frequency was set to 5 Hz. A clip extensometer (MTS 634.11) was used to measure strain data during the entire test. Cameras were placed on each side of the specimen to observe disbond growth from the lateral sides, which were painted with correction fluid. Back-face strain measurements were performed using a fiber optic distributed sensing system based on the Rayleigh Backscattering. The interrogator was an ODiSI-B system from Luna Innovations Inc.[52] (Roanoke, VA, USA) and the sensor comprised of a single mode Ormocer coated low bend loss 125 μm fiber commercialized by FBGS Technologies GmbH (Jena, Germany) with LC/APC connector. The system allows for obtaining strain measurements with 0.65 mm gage pitch along a 10 meter fiber with a maximum data acquisition frequency of 23.8 Hz. The optical fiber was glued to both faces of the specimen in order to capture all the four disbonds, as depicted in Figure 2. Then, five regions of interest were chosen to capture strain measurements, as shown in Figure 2. The camera and fiber optics measurements were taken every 5,000 cycles after stopping the test at the maximum load for a couple of seconds. After the fatigue tests, an ultrasonic inspection was performed with a customized water-jet C-scan system from the Delft Aerospace Structures and Materials Laboratory (DASML). The system is comprised of flat-faced transducer and receiver with nozzle diameter of 8 mm and frequency of 10 MHz.

Numerical model

A finite element model (FEM) was used to obtain the strain distribution on the specimen in order to correlate the strain on the top surface with the disbond tip position. The model was developed in ABAQUS CAE™ using 8-node linear brick C3D8 elements. The model overall dimensions were the same as the tested specimen. The assigned material properties can be found in Table 1. The

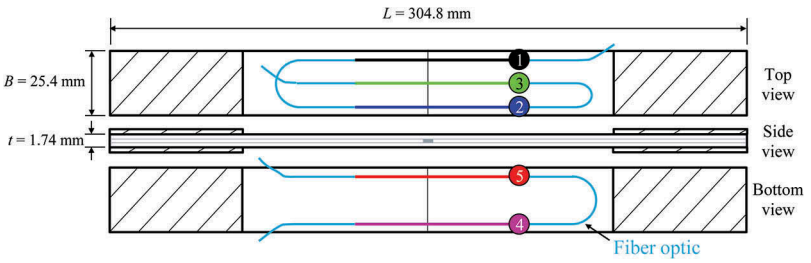

Figure 2. Schematic representation of fiber optics placement on both top and bottom surfaces of the CCP specimen and the 5 regions of interest for measurements.

element size was defined in order to ensure at least one element per composite ply. A convergence study was performed by decreasing element size and no large variations on results were observed. The adhesive layer was modeled with minimum of two elements through thickness so that disbonds could be simulated in the middle interface. The interfaces between composite and adhesive presented tie constraints. Some rows of elements in the adhesive middle interface were modeled with contact properties in order to simulate the disbonds, as depicted in Figure 3. The disbonds were simulated by applying surface-to-surface contacts and small sliding formulation. The tangential contact property was a penalty friction formulation with coefficient 0.2. Simulations were performed with the friction coefficient varying from 0.0 to 0.4 and the variations observed in the results were negligible. The normal contact behavior was defined as "hard" contact with penalty constraint enforcement method with stiffness factor of 1. A load of 42 kN was applied to simulate the maximum load of the fatigue cycle. The FEM consisted of a total of 97,234 C3D8 elements for a total number of 426,135 variables in the problem.

Analytical approach

The expression for calculating the strain energy release rate of the CCP specimen is shown in Equation (1) and it was initially obtained by Wisnom[19], following the approach defined by Williams.[30] Its deduction was explained more in depth by Allegri et al.[22] The model uses classical beam theory and it assumes an unloaded state for the central cut plies in the region where the disbonds are developed. Another assumption is a symmetric disbond growth with respect to the specimen mid-plane. Additionally, Equation (1) is not valid at the vicinity of the disbond tip, where the boundary conditions of the problem are established.[20,25]

For a fatigue test under load control condition, the load variation ΔP, defined by $\Delta P = P_{max}(1 - R)$ on each cycle, results in a ΔG given by Equation (5), obtained after applying Equation (1) on Equation (3). Considering a specimen with a

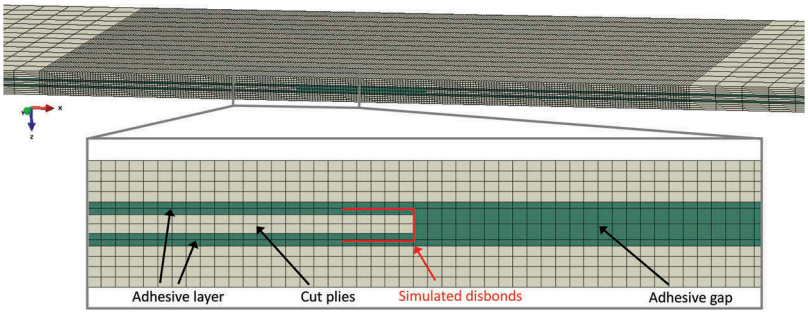

Figure 3. 3D finite element model of the CCP specimen and detailed side view.

defined material and geometry, Equation (5) shows the need to change the fatigue load ΔP in order to obtain different values for ΔG, which are necessary to calculate the parameters of the disbond growth curve defined in Equation (2). It also shows that some geometric parameters or mechanical properties will influence the resulting ΔG differently, being directly or inversely proportional and sometimes to its square value. Nevertheless, there are other parameters that can influence the specimen performance and their influence is not apparent in Equation (5). For instance, the composite tensile strength (σ_{TS}) will determine the maximum load for the fatigue test. Consequently it will limit the maximum ΔG achieved with a defined geometry and material. Thus, the portion of the disbond growth curve defined by higher ΔG values might not be obtained with this specific specimen's geometry. This portion is near the critical mode II strain energy release rate (G_{IIC}), which is another parameter that influences the test performance considerably. An increase in G_{IIC} means increased resistance on disbond development and growth. Consequently, there will be an impact on the disbond growth curve from Equation (2) since more energy will be required to grow the disbond.

$$\Delta G = \left(\frac{\chi}{1-\chi}\right)\frac{{P_{\max}}^2(1-R)^2}{4EB^2t} \tag{5}$$

The specimen's geometry and material properties will also determine the failure type during static tests. The tensile failure can occur in the composite when the stress on the disbonded part of the continuous plies reaches the composite tensile strength. So the failure tensile load (net-section) in the composite adherend ($P_{f,ADHD}$) will be given by σ_{TS} multiplied by the cross-sectional area of the continuous plies. The resulting expression is given by Equation (6). Another option is a disbonding failure, which is a cohesive failure within the adhesive layer. In this case, the failure load for the adhesive ($P_{f,COH}$) can be obtained by substituting G for G_{IIC} in Equation (1). The final expression for $P_{f,COH}$ is shown in Equation (7).

$$P_{f,ADHD} = \sigma_{TS}(1-\chi)Bt \tag{6}$$

$$P_{f,COH} = 2B\sqrt{tEG_{IIC}\left(\frac{1-\chi}{\chi}\right)} \tag{7}$$

Results

Disbond growth measurements

Test results

One of the major issues faced during the fatigue tests was the long test duration. The resulting disbond growth rates were too small and, consequently, the tests needed a high amount of cycles to observe the trends on

disbond growth behavior for the chosen specimen configuration. Strain distributions along the specimen's top and bottom surfaces were measured every 10,000 cycles with a distributed fiber optics sensing system during the fatigue tests. Thus, as the disbonds were growing, changes were observed in the strain profiles for each of the five regions defined in Figure 2. The evolution of the strain distributions on the top surface of the specimen at different fatigue cycle count are shown in Figure 4. In this graph, the position of the adhesive gap is indicated as well as a chosen strain level and the distance of $2a$. This distance is assumed to be the distance between each disbond tip. The assumed disbond length of $2a$ is used in the strain level technique, which is explained in section 4.1.

Unfortunately, during our experimental campaign, the measurements of disbond length through visual inspection of the lateral side of the specimen were not consistent. The white spray paint did not work properly as a result of the thick paint layer applied during the application process, thus not indicating the actual location of the disbonds. It is believed that this was due to the low brittleness level of the paint. Subsequent specimens were painted with correction fluid which worked better. However it was difficult to obtain consistency on the method. Although it was brittle enough to crack under mode II condition, there is a need to obtain a uniform layer over the surfaces in order to observe the disbond growth. In many occasions, a local thicker layer obstructed observation of the disbond length due to the potential of disbond growth under the correction fluid. Thus, the visual inspection with cameras could not be used as an alternative measuring technique for the tests performed.

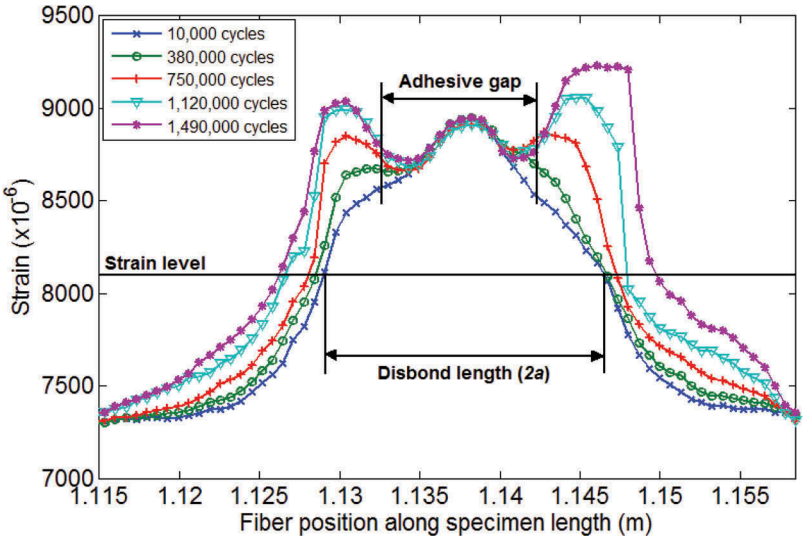

Figure 4. Evolution of strain distribution for one region of the CCP specimen.

A clip extensometer was used to measure the strain over the specimen length. As described in section 2.1, the strain data can be used to calculate the disbond growth rate of the specimen through Equation (4). Figure 5 shows strain data collected at each cycle with the clip extensometer.

After the fatigue tests, the specimens were analyzed with ultrasonic C-scan. Figure 6 shows a C-scan image with the disbonds shown in black in the center of the specimen and a schematic of the optical fiber used on the surface. Thus, a comparison was made with the final measurement of strain distribution at two opposite edges (regions 4 and 5) after the fatigue test and the apparent locations of disbond tips observed from the C-scan. The results can be seen in Figure 6. The disbond tip locations are indicated as a region in the graph due to the low resolution of the C-scan image, which made it difficult to identify the exact tip locations.

Static tests were performed in order to obtain the maximum load (P_{max}) and, consequently, the maximum strain energy release rate ($G_{II,max}$) for this specimen configuration. Some specimens were tested with no pre-disbond while other specimens were tested after the fatigue test with already formed disbonds. The test results presented an average value of 88,736 ± 1,546 N for P_{max}, resulting in a value of 3,496 ± 188 J/m^2 for $G_{II,max}$. The CCP specimen failed abruptly during the static test showing typical behaviour of unidirectional composite failure under tension loading. The calculated value of $G_{II,max}$ is smaller than the G_{IIc} for this specimen configuration, which indicates a possible failure of the composite adherend instead of expected cohesive failure of the adhesive.

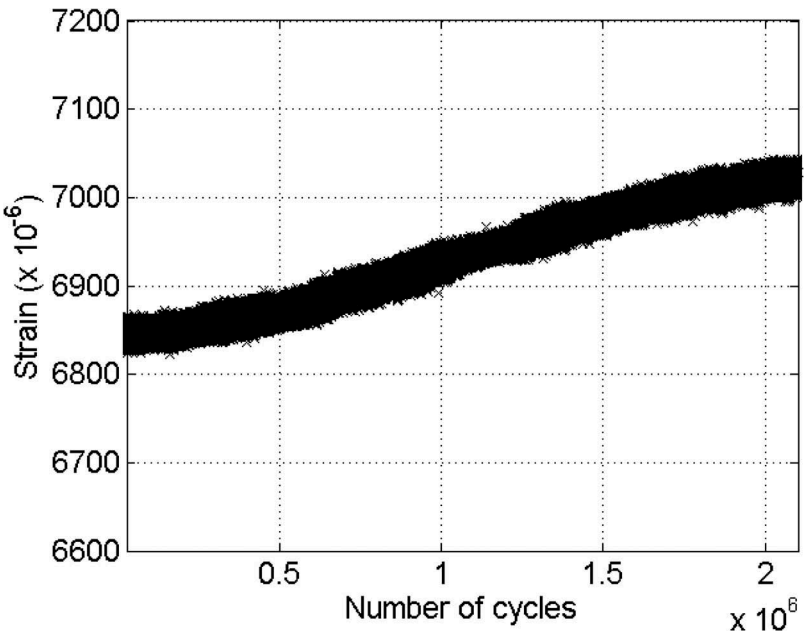

Figure 5. Strain measured with clip extensometer during constant fatigue loading (P_{max} = 42 kN, R = 0.1).

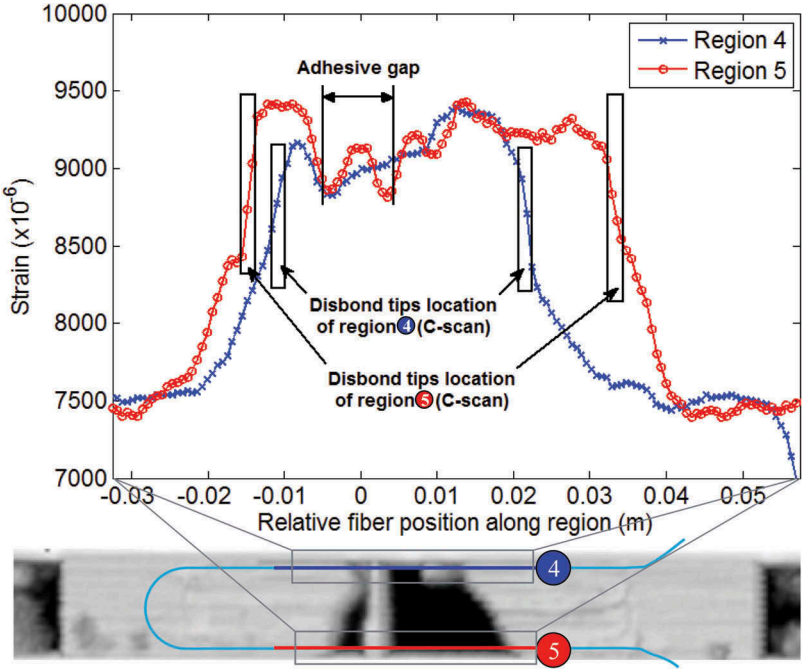

Figure 6. Strain distribution for regions 4 and 5 of the optical fiber after fatigue test and correlation with an image of C-scan inspection.

Finite element model results

A Finite Element Model (FEM) was used to obtain the specimen's strain distribution when subjected to the maximum load. The model simulated disbonds by changing the contact properties of the adhesive layer's middle surfaces from tie constraint to surface contact. Figure 7 shows the results of longitudinal strain (ε_1) for the case where four disbonds of 4 mm are simulated. The strain values shown in Figure 7 are restricted from 0 to 10,000 microstrain in order to allow the observation of strain variations, although values out of this range are found close to the disbond tips (light and dark gray areas). From the results, strain distributions at the top surface of the continuous plies were obtained over the centerline, as indicated in Figure 7. Thus, as the disbonds were propagated, the strain profiles developed as shown in Figure 8, where half specimen is represented due to symmetry. The location of the disbond tip in relation to the top surface's strain profile is indicated with black 'x' markers in the graph.

The results from Figure 8 show very clearly distinct regions. For all cases, the strain value is approximately 9,000 microstrain in the middle section of the specimen, over the adhesive gap. Then the strain decreases reaching a region with a small plateau at a value slightly higher than 8,500 microstrain. Finally, the strain decreases smoothly again reaching a far field constant

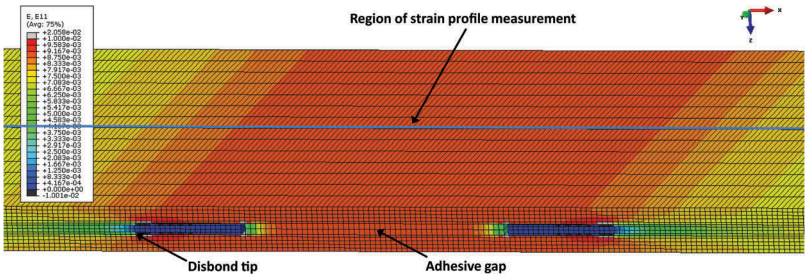

Figure 7. FEM results of longitudinal strain (ε_{11}) for a case of 4 mm disbond lengths with highlighted centerline position for obtaining strain profiles.

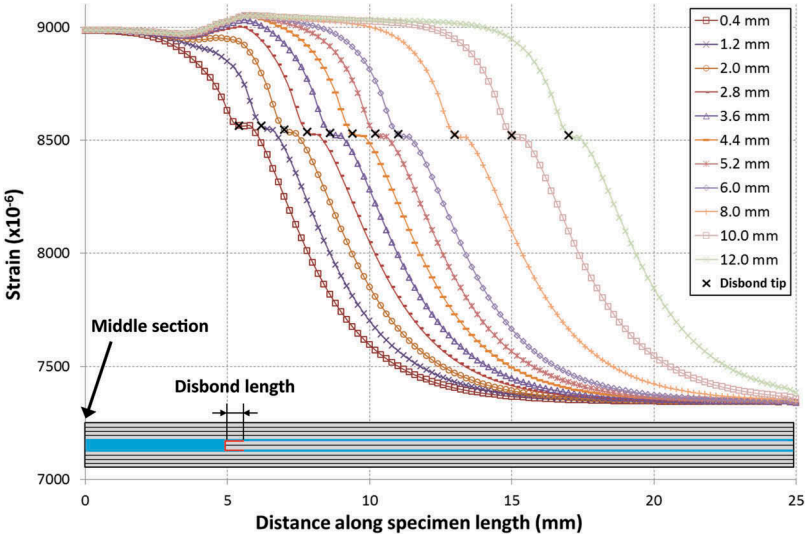

Figure 8. FEM results of longitudinal strain (ε_{11}) distribution over the centerline of specimen's top surface with increasing disbond length.

value around 7,350 microstrain. For disbond lengths smaller than 2.0 mm, the strain value only decreases from the middle section. For longer disbond lengths, a region with local increase in strain value is found right after the beginning of the cut plies and this region grows as the disbond grows. It can be seen that the intermediary plateau advances as the disbond length grows and the actual point on top of the disbond tip is the one just before the plateau.

Study of geometry and material influence

A parametric evaluation of the influence of geometry and material properties on specimen's overall performance and failure mode was executed due to the multiple issues found during the experimental campaign. These issues consisted on: long fatigue test duration, ΔG limitation due to specimen

configuration and adherend failure during static test. The two goals of the parametric evaluation were to avoid adherend failure in static tests and to increase the ΔG range during fatigue testing with the same specimen geometry, thus being able to obtain higher ranges and consequently reduce test duration.

As regards to the static test, a failure ratio was defined as the failure load necessary for the adhesive to fail and the load for net-section failure of the adherends. This failure ratio was obtained by dividing Equation (7) for Equation (6), resulting in Equation (8). Thus, it was possible to evaluate the effect each parameter will have on the failure mode. Figure 9 depicts values of failure ratio with varying cut plies ratio for different thickness. It also assesses the difference between delamination and disbonding condition, considering two different G_{IIC} values from the literature.[53,14] Figure 9(b) clearly shows that the failure mode will change from adhesive failure to adherend failure for every specimen with thickness smaller than 2 mm if a disbonding condition is tested instead of delamination.

$$\frac{P_{f,COH}}{P_{f,ADHD}} = \frac{2}{\sigma_{TS}}\sqrt{\frac{EG_{IIC}}{(1-\chi)\chi t}} \tag{8}$$

For the fatigue tests, it is desirable to achieve a high maximum ΔG with the defined geometry so that by changing the load cycle, different ranges of ΔG can be tested. The ΔG obtained in a fatigue cycle is described by Equation (5). In order to avoid adherend failure, the maximum load will be considered to be a fraction of $P_{f,ADHD}$ defined by λ. Hence $P_{max} = \lambda P_{f,ADHD}$, where λ is smaller than 1. Considering a fatigue cycle with load ratio R, the minimum load is given by $P_{min} = RP_{max}$. Substituting the maximum and minimum loads in Equation (5) and applying Equation (6), the resulting ΔG is given by Equation (9).

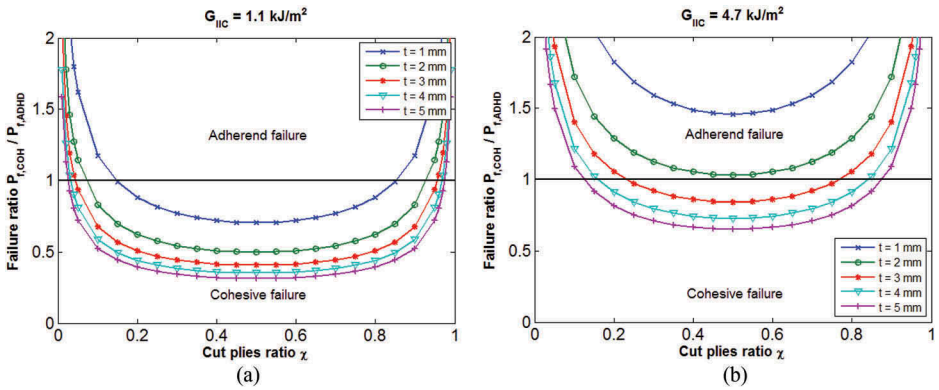

Figure 9. Effect of cut plies ratio and thickness on static failure for carbon/epoxy CCP specimen in case of (a) delamination (G_{IIC} = 1.1 kJ/m^2); (b) disbonding (G_{IIC} = 4.7 kJ/m^2).

$$\Delta G = \frac{(1-R)^2\lambda^2{\sigma_{TS}}^2(1-\chi)\chi t}{4E} \tag{9}$$

Equation (9) shows that the ΔG is independent of G_{IIC}. Thus the ΔG level for the case of composite delamination or disbonding of adhesive joints will be the same if the same material and geometry are considered. Consequently, the reason why a disbonding test with the CCP specimen may take longer than a delamination test to grow for the same defect size is related to the change in the coefficients C and n of the Paris-Erdogan relation given by Eq (2). It can also be concluded that G_{IIC} has a large influence in static tests with this specimen, changing the possible failure mode.

Now consider Equation (9) being applied to the current CCP specimen design, manufactured from carbon/epoxy with material properties E = 156 GPa and σ_{TS} = 2354 MPa, tested under a fatigue cycle with maximum load of 70% of tensile composite failure load (λ = 0.7) and R = 0.1. The resulting ΔG can be seen in Figure 10 with varying cut plies ratio and thickness.

Another parameter to affect the resulting ΔG for a specimen configuration is the material. Equation (9) shows that the ΔG value is inversely proportional to the value of E and directly proportional to the square of σ_{TS}. Although a stronger material can reduce the ΔG value due to its higher elastic modulus, it can also increases ΔG through its higher tensile strength. The impact of changing the material from glass/epoxy to carbon/epoxy is

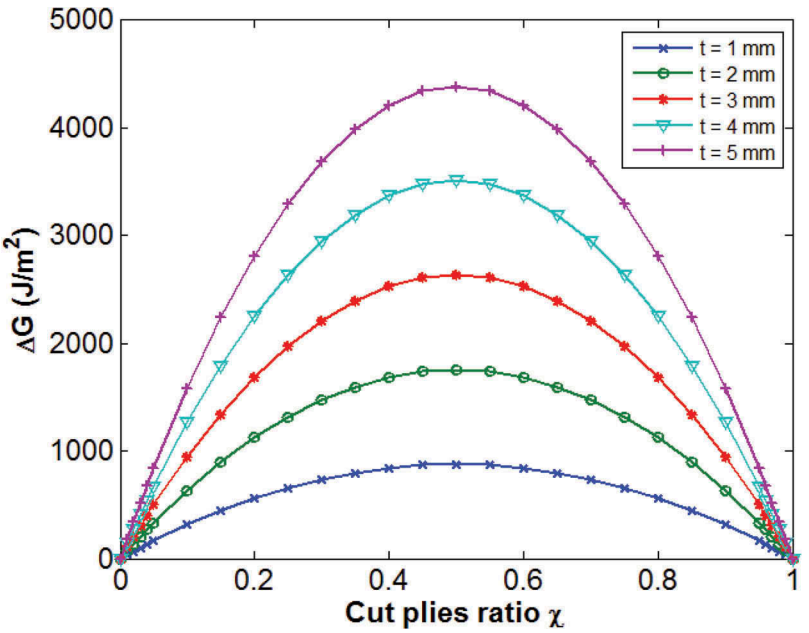

Figure 10. Effect of cut plies ratio and total thickness on maximum ΔG achievable.

Table 2. Effect of different materials on CCP specimens with same geometry and loading.

Material	Tensile Strength, σ_{TS} (MPa)	Young Modulus, E (GPa)	Difference on E (%)	σ_{TS}^2/E (MPa)	Resulting difference on ΔG (%)
Glass/epoxy[20]	1021	43.9	-	23.75	-
Carbon/epoxy[20]	1607	138.0	+214.4	18.71	−21.2

presented on Table 2 using material data from Cui et al.[20] It can be seen that even with an increase of 214.4% in the Young modulus, the final ΔG for a defined geometry and fatigue cycle loading condition is 21.2% smaller.

Discussion

Disbond length determination

The measuring of disbond length is extremely difficult to be performed on a pure mode II fatigue test and different attempts were taken during fatigue tests using cameras and a distributed fiber optic sensing system. In fatigue tests, the common approach is to observe the disbonds from the white-painted lateral face of the specimen with a high definition camera or travelling microscope. Attempts on using this approach with a white spray paint or correction fluid were unsuccessful. In the case of the spray paint, the ductile behavior of the paint did not allow it to break following the specimen's disbond. For the correction fluid, it was easier to observe the disbonds. However, it was necessary to have a really thin and uniform layer throughout the observation area otherwise, in a thicker layer region, the disbond will grow under the correction fluid obstructing its observation. Another downside of the disbond length measurement through lateral face observation is that an unequal crack growth through width cannot be observed if only one lateral face is used. It is necessary to measure both sides.

Alternatively, the strain profiles obtained from the specimen's top and bottom surfaces were used as a means to locate the disbond tip position. It was proposed to study the evolution of the strain distribution over the specimen's external surfaces, which are affected by the growth of each disbond. When the disbonds develop in the adhesive layers, the specimen presents a new load path consisting of mainly the external continuous composite plies. Consequently, the stress and strain levels at the continuous plies increase exactly above the disbonded region. This increase and further development of higher strain values over the continuous plies is related to the disbond growth and the strain profiles were captured by the distributed fiber optic system. Although an evolution in the profile shape is observed in Figure 4, it was unclear how the disbond tip locations are related to the strain distribution.

Therefore, a comparison was made between C-scan measurement after the fatigue test and the last measurement of the distributed sensing fiber optics system, as shown in Figure 6. However, the C-scan measurement resolution was not sufficient to clearly identify the exact location of the disbond tip. As a consequence, a finite element model was used to correlate the disbond tip location to the strain profiles. It was observed in Figure 8 that the disbond tip is located directly below the initial part of a local plateau in the strain profile, typically found around 8,500 microstrain for the considered test case. Similar behavior was observed in the test results from the fiber optics, as can be seen in Figure 4 and Figure 6. However, the strain level in which these local variations were found in the test results varied between 7,900 to 8,400 microstrain. This behavior was observed in some of the fiber optic measurements and it could not be observed in every strain profile due to the resolution of the fiber optic system. The distance between strain measurements for the fiber optic system was 0.65 mm, while the FEM indicated that the local plateau has the same order of magnitude. It is important to note that the fiber optic system is only able to measure strain along the length of the fiber. Even so, the results from the optical fiber when compared with the C-scan and the FEM confirmed that the local plateau in the strain distribution indicates the location of the disbond tip. As a result, the strain profiles obtained at different positions along the specimen allowed the identification of unequal disbond growth which also facilitated the calculation of disbond growth rate through a constant strain level technique.

Disbond growth behavior

The average disbond growth rate was calculated with the data from the clip extensometer and compared to the values obtained with a new methodology using distributed strain measurements. From the clip extensometer results shown in Figure 5 and using Equation (4), the disbond growth rate obtained was 3.98×10^{-6} mm/cycle. It is important to notice that the clip extensometer is capturing the strain for the whole central part of the specimen and the proposed methodology considers the four disbonds growing equally. Thus, the result is an average disbond growth rate for the four disbonds.

The strain profiles obtained from the optical fiber distributed on both surfaces of the specimen (Figure 2) were used to investigate individual disbond growth. Although the local plateau of strain distribution could not be found in every strain profile, a strain level technique was used to calculate disbond growth for each region. The technique consisted in defining a strain level and measuring the distance between the two points where the strain profile cross that strain level. This distance is assumed as the double of the disbond length ($2a$), since it goes from one disbond tip to another one. Figure 4 shows one example of a chosen strain level and the calculated

distance 2*a*. Next, disbond growth curves were obtained for each fiber region for a strain level of 8,200 microstrain and the results are shown in Figure 11. Each curve relates to one of the five regions of the optical fiber, as indicated next to the graph. Corresponding disbond growth rates for each region were calculated from the slope of each curve.

The results indicate an unequal disbond growth in the specimen. The disbond growth curves present different rates along the specimen's width. Regions 1 and 4 are located in opposite surfaces through thickness and on the same edge of the specimen. However, regions 2 and 5 are located on the opposite edge of the specimen. Region 3 is located in the centerline of the specimen's top surface. The curves of Figure 11 indicate disbonds growing slower in one edge (regions 1 and 4), faster in the center (region 3) and even faster in the opposite edge (regions 2 and 5), which was confirmed by the image of the ultrasonic C-scan inspection. These curves also indicated that the disbonds directly opposite to each other with respect to the thickness were growing at a similar rate. This is indicated by the curve of region 5 being practically on top of region 2 and by the curve of region 1 and 4 being really close to each other as shown in Figure 11. The small difference between curves of regions 1 and 4 can be a result of 1 mm difference in fiber placement position. While region 1 was located 3 mm away from the edge, region 4 was located 2 mm away from the edge, which can generate the small difference between the curves.

The unequal disbond growth and also the chosen strain level will influence the final calculated disbond growth rate for the specimen. While the FEM results showed the disbond tips being located around a strain level of 8,500 microstrain,

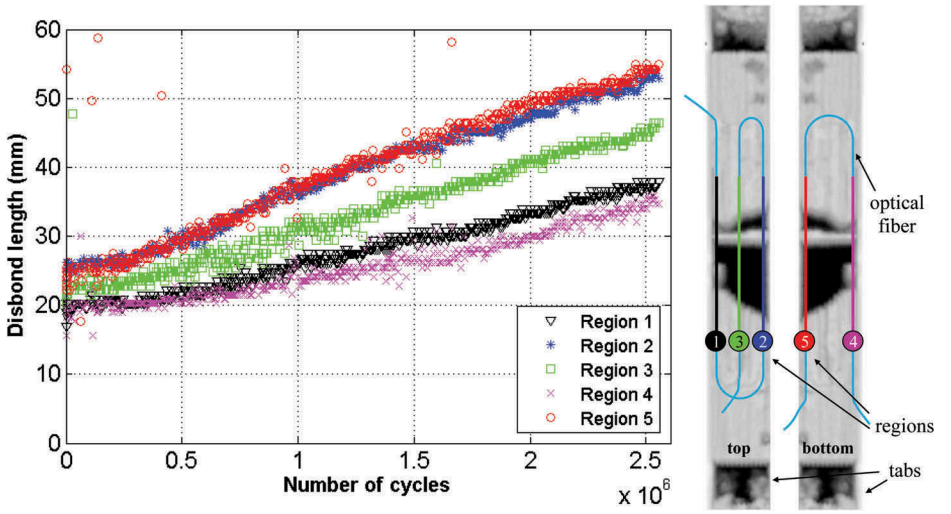

Figure 11. Disbond growth curves from five regions obtained with a strain level of 8200 με and C-scan top and bottom surface images with corresponding measurement regions.

experimentally it was difficult to locate them due to the resolution of 0.65 mm of the fiber optic system. Thus, in order to calculate the disbond growth, a fixed strain level was chosen for the calculation. The influence of the different strain levels and the influence of the unequal disbond growth were investigated. Figure 12 shows the disbond growth rates calculated with the strain level technique obtained at different strain levels and for two fiber regions, 1 and 2, located at opposite edges. The obtained result from the clip extensometer measurements was calculated and shown in the figure for comparison. The chosen strain levels were between 7,900 to 8,400 microstrain, which is the range where the slope variations on the strain profiles were found in the experimental campaign.

The results from Figure 12 show small variations on the disbond growth rate in relation to the chosen strain level. For region 1, the average disbond growth rate was 3.08×10^{-6} mm/cycle and the maximum difference between the strain levels was 5.8%. For region 2, the average disbond growth rate was 5.22×10^{-6} mm/cycle and the maximum difference between the strain levels was 3.1%. Thus, it was found that the variation in disbond growth when choosing a different strain level is small. The experimental results indicated that the local plateau in the strain profiles was more frequently occurring around 8,200 microstrain, which is about half way between the top and bottom strain values of 7,350 and 9,000 microstrain from the far field and disbonded regions respectively. Figure 12 also shows the average disbond growth rate calculated with the clip extensometer. It can be seen that the value is consistent and comprises of an average between the opposite specimens edges.

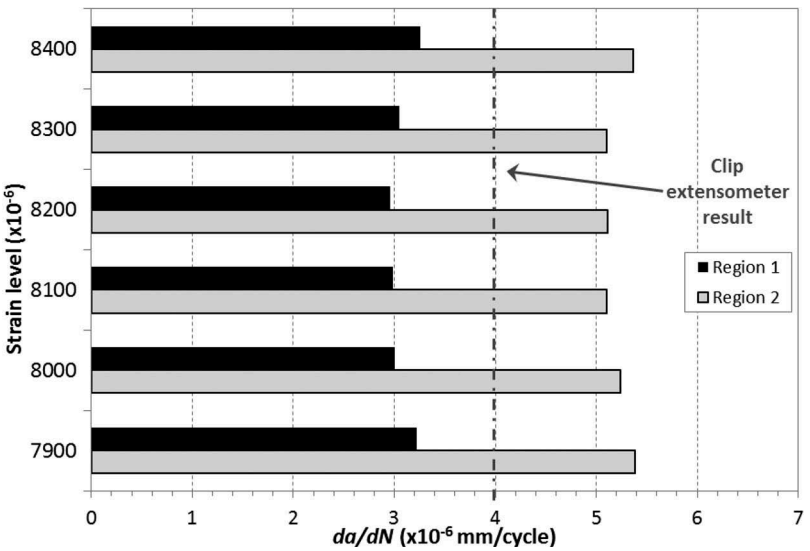

Figure 12. Disbond growth rates obtained with the strain level technique at opposite edges of the specimen (regions 1 and 2 of the optical fiber sensor).

Considerations for disbonding vs. delamination

A big difference in specimen performance was observed when the same geometry was used for disbonding fatigue tests instead of delamination tests, related mainly to the large difference in mode II critical strain energy release rate (G_{IIC}). The first problem was the long test duration, consequence of an extremely low disbond growth rate. The results were completely different from previous work[23] on delamination of CCP specimens with similar configuration (2 cut/8 continuous plies) using the same materials. The higher G_{IIC} of the disbonding CCP specimens results in higher resistance for the disbonds to develop between the cut and continuous plies. Thus, for the same ΔG level, a delamination CCP specimen will present a higher fracture growth rate than a disbonding CCP specimen. And the lower fracture growth rate of the disbonding case makes the fatigue test duration longer.

One option to address this problem could be an increase in test frequency. Nevertheless, this option was not cogitated since 5 Hz is already considered a limit frequency to test resin dominated laminates and higher frequencies can lead to problems related to hysteretic heating of the adhesive.[54] Consequently, there was a need to increase ΔG and reach higher values of da/dN. In addition, it is important to be able to obtain the full da/dN vs. ΔG curve for this material. The problem is the limitation in the increase of ΔG for a chosen CCP specimen geometry. According to Equation (5), the only way to increase ΔG for a defined material, geometry and load ratio is to increase the maximum load. However, the higher load can lead the failure to occur in the adherend first.

In this way, it is desirable to avoid failure in the adherend, letting a delamination or disbonding critical condition to occur first. The specimen geometry and the G_{IIC} will influence the failure mode. Figure 9 demonstrates that the static failure for a chosen total thickness and cut plies ratio could change from failure within the adhesive to failure within the adherend when G_{IIC} is increased from the delamination case (lower G_{IIC}) to the disbonding case (higher G_{IIC}). By analyzing Figure 9 with the typical CCP geometry from literature with a cut plies ratio of 0.2 and total thickness between 1 and 2 mm, it can be seen that the increase in G_{IIC} by the addition of adhesive layers changes the static failure from occurring in the adhesive to befalling in the adherends. This was the case observed in the static tests performed with the current material and geometry.

Furthermore, material properties can also affect the ΔG obtained in fatigue tests. Equation (9) showed that ΔG is directly proportional to the ratio between the square of the tensile strength and the elastic modulus. As a result, a CCP specimen manufactured with a material that has a high tensile strength and low elastic modulus can withstand a higher ΔG. Table 2 showed that a CCP specimen with same geometry and loading conditions can present a higher ΔG with glass/epoxy than with carbon/epoxy, which is a stronger

material. The important point about material selection is also to avoid adherend failure and it is noted that a stronger material will not necessarily allow a higher ΔG with the CCP specimen.

It was also shown through this study the importance of a proper choice of cut plies ratio and thickness (or plies quantity) to achieve a higher range of strain energy release rate (ΔG) and distinct values of disbond growth rate that allows more data to be obtained for the *da/dN* vs. ΔG curve, as seen in Figure 10. It was verified that the typical 2 cut/8 continuous plies configuration commonly used for delamination studies was not optimized for obtaining a wider range of ΔG, especially for a bonded specimen. The maximum load was limited to avoid adherend failure. As a consequence, the *da/dN* vs. ΔG curve was not obtained with this specimen configuration, since it required higher loading to obtain more data points. In order to avoid such issue, an improved CCP specimen with a cut plies ratio of 0.5 should be considered.

Conclusions

The Central Cut Plies (CCP) specimen is a good alternative for mode II fatigue testing of composite materials. This work indicates that the specimen can be used for the evaluation of bonded joints in addition to the delamination studies already found in literature. However, for each case, the specimen's geometry should be optimized for better results. The specimen's characteristics of producing a constant disbond growth when a constant amplitude tensile loading is applied under load control, in addition to its stable disbond growth makes it advantageous for mode II fatigue studies, avoiding, for example, stability problems faced with the End Notched Flexure (ENF) specimen. Though, the choice of specimen's material and geometry are important and should be defined accordingly to avoid adherend failure along with guaranteeing a large range of strain energy release rate (ΔG) during the fatigue tests. This study showed that a cut plies ratio of 0.5 seems to be an optimum value when using the CCP specimen.

A big advantage of the CCP specimen is the possibility of obtaining the average disbond growth rate with the use of a clip extensometer, avoiding the typical inaccurate visual measurements involving mode II specimens. Disbond length measurements taken from visual inspection of the lateral face of the specimen proved to be unreliable and the presence of unequal disbond growth through the width highlights the need of observing both lateral faces. For the identification of unequal growth and calculation of each individual disbond growth, a new technique using distributed strain measurements was demonstrated for this application. The technique revealed to be reliable in calculating disbond growth and allowed for good estimation of disbond tip location. Both clip extensometer and distributed strain sensing

techniques presented good correlation with ultrasonic C-scan results, even when unequal disbond growth along the specimen's width was observed. The correlation between surface strain measurements and disbond tip location was confirmed with finite element model simulation.

Acknowledgments

The authors would like to acknowledge the funding received for this project through the Brazilian Air Force and the FP7 Marie Curie Career Integration Grant titled 'Monitoring of Aerospace Structural Shapes - MASS' (Project ID 618316). In addition, the authors would like to thank the technical advice and support given by Dr. Chun Li at the National Research Council of Canada.

Funding

This work was supported by the FP7 People: Marie-Curie Actions (Project ID 618316).

ORCID

Fabricio N. Ribeiro http://orcid.org/0000-0002-3979-5360
Marcias Martinez http://orcid.org/0000-0002-3985-9926
Calvin Rans http://orcid.org/0000-0001-5539-1262

References

[1] Flinn, R. A.; Trojan, P. K. *Engineering Materials and Their Applications*, 4th ed.; Wiley: New York, 1995; pp 608.
[2] Baker, A.;. *Trans. Ins. Eng. Aus. Mech. Eng.* 1996, *21*(1–2), 1–59.
[3] Baker, A.;. *Compos. Struct.* 1999, *47*(1), 431–443. DOI: 10.1016/S0263-8223(00)00011-8.
[4] Federal Aviation Administration. *Composite Aircraft Structure*; AC 20-107B; 2009.
[5] Hart-Smith, L. J. NASA Contract Rep CR-2218; 1974.
[6] Marissen, R. Doctoral thesis, Technische Universiteit Delft, The Netherlands, 1988.
[7] Rans, C. D.; Alderliesten, R. C. In *ICAF 2009 Bridging the Gap between Theory and Operational Practice*. Bos, M. J., Eds.; Springer: Dordrecht, Netherlands, 2009; pp 73–90.
[8] Hiley, M. J.;. *Plast. Rubber Compos.* 1999, *28*(5), 210–227. DOI: 10.1179/146580199101540358.
[9] Bürger, D. Doctoral thesis, Technische Universiteit Delft, The Netherlands, 2015.
[10] Davies, P.; Blackman, B. R. K.; Brunner, A. J. *Appl. Compos. Mater.* 1998, *5*, 345–364. DOI: 10.1023/A:1008869811626.
[11] Davies, P.; Sims, G. D.; Blackman, B. R. K.; Brunner, A. J.; Kageyama, K.; Hojo, M.; Tanaka, K.; Murri, G.; Rousseau, C.; Gieseke, B.; Martin, R. H. *Rubber Compos.* 1999, *28*(9), 432–437. DOI: 10.1179/146580199101540600.
[12] Davies, P.; Blackman, B. R. K.; Brunner, A. J. In *Fracture Mechanics Testing Methods for Polymers, Adhesives and Composites*, Moore, D. R., Pavan, A., Williams, J. G., Eds.; ESIS Publication 28, Elsevier: Amsterdam, 2001; pp 307–334.

[13] Brunner, A. J.; Blackman, B. R. K.; Davies, P. *Eng. Fract. Mech.* 2008, *75*, 2779–2794. DOI: 10.1016/j.engfracmech.2007.03.012.
[14] de Moura, M. F. S. F.; Campilho, R. D. S. G.; Gonçalves, J. P. M. *Int. J. Solids Struct.* 2009, *46*(6), 1589–1595. DOI: 10.1016/j.ijsolstr.2008.12.001.
[15] ASTM D7905/D7905M-14. *Standard Test Method for Determination of the Mode II Interlaminar Fracture Toughness of Unidirectional Fiber-Reinforced Polymer Matrix Composites*; ASTM International: West Conshohocken, PA, 2014.
[16] Kageyama, K.; Kikuchi, M.; Yanagisawa, N. In *Composite Materials Fatigue and Fracture*, O'Brien, T. K., Ed.; ASTM STP 1110, American Society for Testing Materials: Philadelphia, 1991; Vol. 3rd, pp 210–225.
[17] Martin, R. H.; Davidson, B. D. *Rubber Compos.* 1999, *28*(8), 401–406. DOI: 10.1179/146580199101540565.
[18] Blackman, B. R. K.; Brunner, A. J.; Williams, J. G. *Eng. Fract. Mech.* 2006, *73*(16), 2443–2455. DOI: 10.1016/j.engfracmech.2006.05.022.
[19] Wisnom, M. R.;. *J. Reinf. Plast. Compos.* 1992, *11*(8), 897–909. DOI: 10.1177/073168449201100802.
[20] Cui, W.; Wisnom, M. R.; Jones, M. *J. Reinf. Plast. Compos.* 1994, *13*(8), 722–739. DOI: 10.1177/073168449401300804.
[21] Wisnom, M. R.; Jones, M. I.; Cui, W. *Astm Stp*. 1995, *1230*, 486–508.
[22] Allegri, G.; Jones, M. I.; Wisnom, M. R.; Hallett, S. R. *Compos. Part A*. 2011, *42*(7), 733–740. DOI: 10.1016/j.compositesa.2011.02.013.
[23] Rans, C. D.; Atkinson, J.; Li, C. *J. Compos. Mater.* 2015, *49*(6), 685–697. DOI: 10.1177/0021998314525482.
[24] Wang, W.-X.; Nakata, M.; Takao, Y.; Matsubara, T. *Compos. Part A*. 2009, *40*(9), 1447–1455. DOI: 10.1016/j.compositesa.2009.04.029.
[25] Kawashita, L. F.; Jones, M. I.; Trask, R. S.; Hallett, S. R.; Wisnom, M. R. *17th International Conference on Composite Materials*; IOM Communications Ltd: Edinburgh, Scotland, 2009.
[26] Van Der Meer, F. P.; Sluys, L. J. *Compos. Part A*. 2013, *54*, 145–152. DOI: 10.1016/j.compositesa.2013.07.013.
[27] Jalalvand, M.; Czél, G.; Fuller, J. D.; Wisnom, M. R.; Canal, L. P.; González, C. D.; LLorca, J. *Compos. Sci. Technol.* 2016, *134*, 115–124. DOI: 10.1016/j.compscitech.2016.08.001.
[28] Scalici, T.; Pitarresi, G.; Catalanotti, G.; van der Meer, F. P.; Valenza, A. *Compos. Struct.* 2016, *158*, 144–159. DOI: 10.1016/j.compstruct.2016.09.033.
[29] Wisnom, M. R. Proceddings of 32nd AIAA Structures, Structural Dynamics and Materials Conference, Baltimore, 1991, pp 1162–1172.
[30] Williams, J. G.;. *Int. J. Fract.* 1988, *36*(2), 101–119. DOI: 10.1007/BF00017790.
[31] Pascoe, J. A.; Rans, C. D.; Benedictus, R. *Eng. Fract. Mech.* 2013, *109*, 150–160. DOI: 10.1016/j.engfracmech.2013.05.015.
[32] Rans, C.; Alderliesten, R.; Benedictus, R. *Compos. Sci. Technol.* 2011, *71*(2), 230–238. DOI: 10.1016/j.compscitech.2010.11.010.
[33] Campilho, R. D. S. G.; Moura, D. C.; Gonçalves, D. J. S.; Da Silva, J. F. M. G.; Banea, M. D.; Da Silva, L. F. M. *Compos. Part. B*. 2013, *50*, 120–126. DOI: 10.1016/j.compositesb.2013.01.025.
[34] Stelzer, S.; Pinter, G. *Mater. Sci. Forum*. 2015, *825-826*, 914–921. DOI: 10.4028/www.scientific.net/MSF.825-826.
[35] Greenhalgh, E. S.;. *Failure Analysis and Fractography of Polymer Composites*; Woodhead Publishing Limited: UK, 2009.

[36] Mall, S.; Kochhar, N. K. *Eng. Fract. Mech.* 1988, *31*(5), 747–758. DOI: 10.1016/0013-7944(88)90231-7.
[37] Blackman, B. R. K.; Kinloch, A. J.; Paraschi, M. *Eng. Fract. Mech.* 2005, *72*(6), 877–897. DOI: 10.1016/j.engfracmech.2004.08.007.
[38] Brussat, T. R.; Chiu, S. T.; Mostovoy, S. AFML-TR-163, Air Force Materials Laboratory, Wright-Patterson AFB: Dayton, 1977.
[39] Mall, S.; Johnson, W. S.; Everett, R. A., Jr., Tech Rep NASA-TM-84577, NASA Langley Research Center: Hampton, 1982.
[40] Wachnicki, C. R.; Radon, J. C. *Composites*. 1984, *15*(3), 211–216. DOI: 10.1016/0010-4361(84)90277-5.
[41] Roy, C.; El Ghorba, M. *Polym. Compos.* 1988, *9*(5), 345–351. DOI: 10.1002/(ISSN)1548-0569.
[42] Zhang, Y.; Keller, T. *Compos. Sci. Technol.* 2008, *68*(2), 461–470. DOI: 10.1016/j.compscitech.2007.06.011.
[43] Habib, F.; Martinez, M.; Artemev, A.; Brothers, M. *Compos. Part. B*. 2013, *47*, 26–34. DOI: 10.1016/j.compositesb.2012.11.002.
[44] Genest, M.; Martinez, M.; Mrad, N.; Renaud, G.; Fahr, A. *Compos. Struct.* 2009, *88*(1), 112–120. DOI: 10.1016/j.compstruct.2008.02.010.
[45] Crocombe, A. D.; Ong, C. Y.; Chan, C. M.; Wahab, M. A.; Ashcroft, I. A. *J. Adhes.* 2002, *78*(9), 745–776. DOI: 10.1080/00218460213835.
[46] Shenoy, V.; Ashcroft, I. A.; Critchlow, G. W.; Crocombe, A. D.; Abdel Wahab, M. M. *Int. J. Adhes. Adhes.* 2009, *29*(4), 361–371. DOI: 10.1016/j.ijadhadh.2008.07.008.
[47] Jones, R.; Galea, S. *Compos. Struct.* 2002, *58*(3), 397–403. DOI: 10.1016/S0263-8223(02)00235-0.
[48] Murayama, H.; Kageyama, K.; Uzawa, K. *Health Monit.* 2011, *11*(3), 325–344. DOI: 10.1177/1475921711419994.
[49] Bernasconi, A.; Kharshiduzzaman, M.; Anodio, L. F.; Bordegoni, M.; Re, G. M.; Braghin, F.; Comolli, L. *J. Adhes.* 2014, *90*(5–6), 496–510. DOI: 10.1080/00218464.2013.857606.
[50] Bernasconi, A.; Carboni, M.; Comolli, L.; Galeazzi, R.; Gianneo, A.; Kharshiduzzaman, M. *J. Adhes*. 2016, *92*(7–9), 739–757. DOI: 10.1080/00218464.2015.1123153.
[51] Wong, L.; Chowdhury, N.; Wang, J.; Chiu, W. K.; Kodikara, J. *Materials*. 2016, *9*(5), 374. DOI: 10.3390/ma9050374.
[52] Luna Innovations Inc. http://www.lunainc.com/product/sensing-solutions/odisi/ (accessed Sep 18, 2017).
[53] Jimenez, M. A.; Miravete, A. *J. Compos. Mater.* 2004, *38*, 1309–1335. DOI: 10.1177/0021998304042734.
[54] Curtis, P. T.;. *J. Strain Anal. Eng.* 1989, *24*(4), 235–244. DOI: 10.1243/03093247V244235.